NANO · MICRO small

www.small-journal.com

Cloaked Exosomes: Biocompatible, Durable, and Degradable Encapsulation

*Sumit Kumar, Issac J. Michael, Juhee Park, Steve Granick, and Yoon-Kyoung Cho**

Exosomes—nanosized extracellular vesicles (EVs) naturally secreted from cells—have emerged as promising biomarkers and potential therapeutic vehicles, but methods to manipulate them for engineering purposes remain elusive. Among the technical obstacles are the small size and surface complexity of exosomes and the complex processing steps required, which reduce the biocompatibility of currently available methods. The encapsulation of exosomes with a nanofilm of supramolecular complexes of ferric ions (Fe^{3+}) and tannic acid is demonstrated here. The resulting natural polyphenol, ≈10 nm thick, protects exosomes from external aggressors such as UV-C irradiation or heat and is controllably degraded on demand. Furthermore, gold nanoparticles can be covalently attached for single-exosome level visualization. To fully exploit their therapeutic potential, chemotherapeutic drug-loaded EVs are functionalized to achieve the targeted, selective killing of cancer cells preferentially over normal cells. This nanofilm not only preserves the native size and chemical makeup of the intrinsic exosomes, but also confers new capabilities for efficient tumor targeting and pH-controlled release of drugs. Demonstrating a scalable method to produce biocompatible, durable, on-demand degradable, and chemically controllable shields for exosome modification and functionalization, the methods introduced here are expected to bring the potential of exosome-based nanomedicine applications closer to reality.

Exosomes are tiny vesicles ranging in size from 30 to 100 nm that mediate intercellular communication by delivering a variety of biomolecules, including proteins, lipids, and nucleic acids.[1,2] Exosomes actively participate to regulate immunomodulation, initiate the formation of premetastatic niches, determine organotropic metastasis for the influx of tumor cells, and confer chemotherapeutic resistance by shuttling genetic molecules among cells.[3,4] Owing to their good correlation with disease status and progression, exosomes are recognized as a potential source of diagnostic biomarkers and therapeutic agents.[5] While their biocompatibility, immunologically inert nature, and nanosized structure might seem to render them promising candidates as nanocarriers for therapeutic applications, in practice, exosomes suffer from limited long-term stability. We were specifically interested in addressing the lack of available methods to modify their surfaces, which could endow exosomes with additional functionalities such as targeting moieties, imaging markers, or synergistic drugs.[6]

Currently, surface engineering of exosomes follows two main approaches: genetic manipulation of parent cells and direct chemical conjugation of the exosomal membrane.[7] However, these methods suffer from intrinsic drawbacks, such as the use of complicated manipulations and the requirement for harsh reaction conditions. The necessity of extreme temperature, pressure, or solvent exposure may cause membrane disruption and surface protein denaturation, while exposure to low or high salt concentrations leads to osmotic stress, which can affect their structure and function of the exosomes.[8,9] Recent reports highlight the loss of exosomes and leakage of exosomal proteins depending on storage conditions.[6] Therefore, the development of a mild, uniform, and biocompatible method for coating individual exosomes with mechanically durable and chemically controllable materials would expand the potential applications of exosome-based theranostics.[6a]

We sought to utilize phenolic-based coatings in which tannic acid (TA) coordinates with Fe^{3+} to form a coordination complex.[10] Such uniform coatings would be attractive for biological applications but cannot be produced using the methods by which they have heretofore been used for cell encapsulation.[11] These procedures require 6 h to coat yeast cells at low pH, and the yeast cells must be fed with Fe^{3+} for 12 h prior to incubation with TA (Tables S1–S3, Supporting Information). In reality, exosomes cannot survive for this long at low pH. In order to coat tiny and fragile exosomes while avoiding aggregation, we used a microfluidic-based droplet generation device (Figure S1, Video S1, Supporting Information). Water-in-oil droplet reactors were produced at a microfluidic T-junction, where two aqueous phases met (at 2 μL min^{-1}) and were delivered into the oil stream (at 150 μL min^{-1}) where they were broken into droplets due to shear forces. One aqueous phase contained exosomes

Dr. S. Kumar, I. J. Michael, J. Park, Prof. S. Granick, Prof. Y.-K. Cho
Center for Soft and Living Matter
Institute for Basic Science (IBS)
Ulsan 44919, South Korea
E-mail: ykcho@unist.ac.kr
I. J. Michael, Prof. Y.-K. Cho
Department of Biomedical Engineering
School of Life Sciences
Ulsan National Institute of Science and Technology (UNIST)
Ulsan 44919, South Korea
The ORCID identification number(s) for the author(s) of this article can be found under https://doi.org/10.1002/smll.201802052.

DOI: 10.1002/smll.201802052

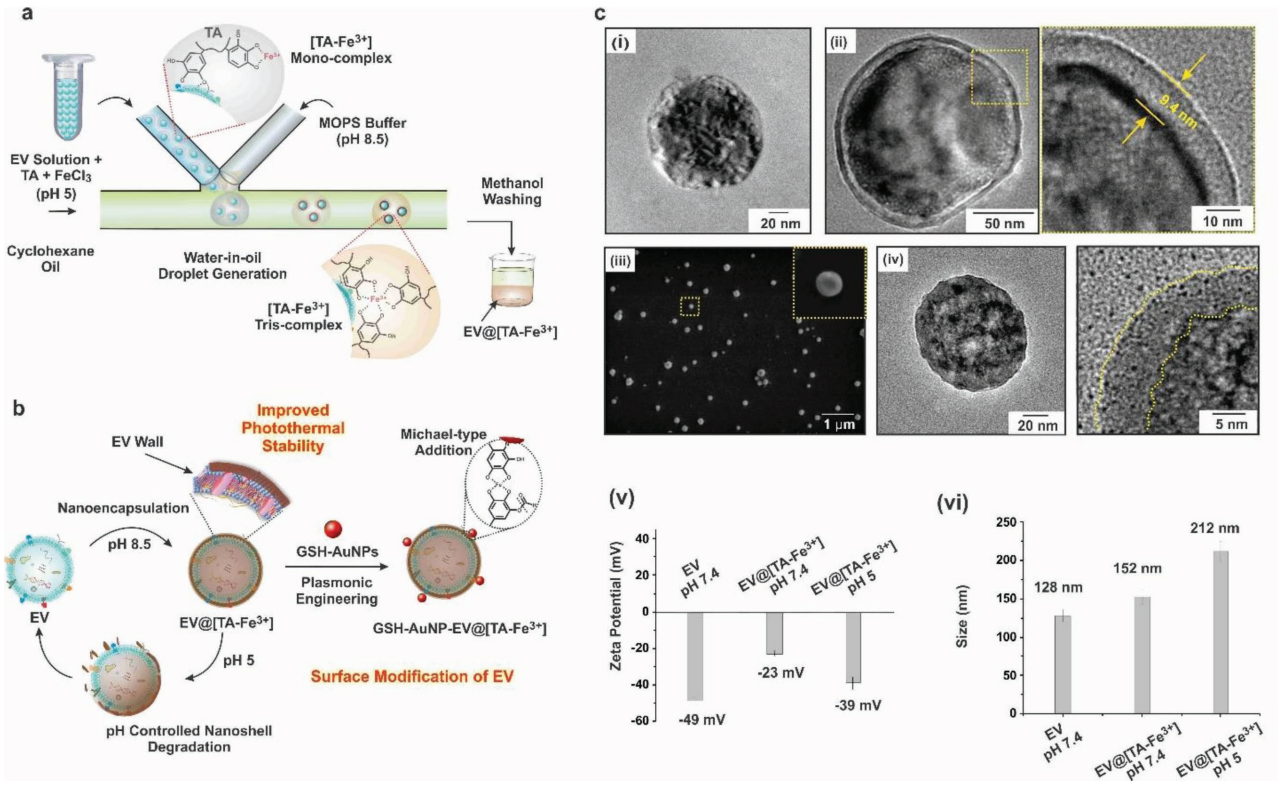

Figure 1. a) Schematic representation of the microfluidic device used to encapsulate individual exosomes. A generic term, EV, was used for all secreted vesicles including exosomes and microvesicles. b) Schematic representation of the pH-controlled formation and degradation of [TA-Fe^{3+}] nanofilms to enhance chemical, thermal, and mechanical stability, as well as surface functionalization with AuNPs to demonstrate the capability of chemical modification. c) Physiochemical characterization: TEM image of (i) EV (pH = 7.4), (ii) EV@[TA-Fe^{3+}] (pH = 7.4), (iii) SEM of EV@[TA-Fe^{3+}] (pH = 7.4), and (iv) TEM image of EV@[TA-Fe^{3+}] (pH = 5); (v) Zeta potential and (vi) size of EV (pH = 7.4), EV@[TA-Fe^{3+}] (pH = 7.4), and EV@[TA-Fe^{3+}] (pH = 5). All values are expressed as the mean ± SD (n = 3 individual experiments).

(5×10^8 particles mL^{-1}, MCF-7 cells), TA (40 μg mL^{-1}), and $FeCl_3 \cdot 6H_2O$ (8 μg mL^{-1}, pH < 5), and the other contained 3-(*N*-morpholino)propanesulfonic acid (MOPS) buffer (pH 8.5) (**Figure 1**a). The pH < 5 of the first phase, caused by the acidity of the $FeCl_3$ solution, produced polyphenol–Fe^{3+} monocomplex emulsions that were then stabilized by increasing the pH with MOPS buffer (pH 8.5) at the T-junction, allowing the pyrogallol (1,2,3-trihydroxy benzene) moiety in TA to act as a bidentate ligand, while Fe^{3+} formed tris complexes.[12] Downstream, we harvested the resulting homogeneous emulsions of extracellular vesicles (EVs) coated with [TA-Fe^{3+}] nanofilm. The thickness of the nanofilm (9.7 ± 0.3 nm, measured from 50 data points in 10 different transmission electron microscopy (TEM) images, Figure S2, Supporting Information), was uniform due to the controlled supply of reactants and efficient mixing in the confined droplet reactor (≈8 nL) (EV size ranging from 40 to 160 nm). The versatility of the biphasic water-in-oil system for nanoencapsulation was also demonstrated by the formation of uniform nanofilms with thickness of 9.0 ± 1.4 nm on AuNPs, measured from 20 data points (Figure S3, Supporting Information) and by the shift in the absorption band in UV-vis spectroscopy from 523 to 526 nm (Figure S4, Supporting Information). A key point of this design strategy was that monodisperse, nanoliter-scale droplet reactors in continuous flow enabled the scalable production of aggregation-free, uniform nanofilm formation on exosomes due to the tight spatial and temporal control of the mixed reactants using the water-in-oil biphasic systems.

Just as when films of this type are used to encapsulate cells,[11] these coatings degraded when the pH was lowered to 5, and they acted as a protective layer from UV-C irradiation and long-term storage at 37 °C (Figure 1b). The versatile surface chemistry allowed us to link glutathione-capped gold nanoparticles (GSH-AuNPs) to the films by esterification; this staining with gold allowed us to visualize them at the single-exosome level using dark-field microscopy (DFM).

To produce the feedstock needed for microfluidics, MCF-7 cell-derived EVs were isolated based on a published protocol and characterized by nanoparticle tracking analysis (NTA) (Figure S5, Supporting Information) and TEM (Figure 1c–i).[13] The presence of the phenolic coating was visible even to the naked eye as the color changed from transparent to purple (Figure S6, Supporting Information). When the flow rate of cyclohexane was reduced to 25 μL min^{-1} for visualization, a color change from transparent to bluish-black and efficient mixing within the droplets could be observed in <1 s (Figure S1e, Video S2, Supporting Information), suggesting that the reaction occurred almost instantaneously. Their thickness and uniformity were characterized by TEM (Figure 1c–ii; Figure S2, Supporting Information) and scanning electron microscopy (SEM) images (Figure 1c–iii),

and the presence of the coordination complex was confirmed by Raman spectroscopy (Figure S7, Supporting Information) and UV–vis spectroscopy (Figure S8, Supporting Information).[11] When the concentration of TA was kept low at 40 μg mL^{-1} (0.024×10^{-3} M), and the Fe^{3+}/TA molar ratios were varied from 1:1 to 1:4, the nanofilm thickness, measured from 20 data points, remained uniform (Figure S9, Supporting Information).

The degradation of the nanofilm at low pH was confirmed using TEM (Figure 1c–iv), Raman spectroscopy (Figure S7, Supporting Information), and UV–vis spectroscopy (Figure S8, Supporting Information). We also confirmed the presence of Fe^{3+} in the nanofilm by adding ethylenediaminetetraacetic acid (EDTA) (Figure S10, Supporting Information). The intensity of the UV–vis band at 546 nm decreased with increasing EDTA concentration because of its strong affinity for Fe^{3+}, which resulted in the gradual disassembly of the [TA-Fe^{3+}] nanofilm. In addition, the dynamic light scattering (DLS) analysis of EV@[TA-Fe^{3+}] showed a less negative charge (–23 ± 1.6 mV, three individual experiments) than the uncoated exosomes (–49 ± 1.2 mV, three individual experiments), indicating the presence of galloyl (trihydroxyphenyl) groups (Figure 1c–v). After decreasing the pH to 5, the zeta potential changed to −39 ± 3.4 mV (three individual experiments) due to the disassembly of the nanofilm. The average size of the exosomes increased from 128 ± 3.6 to 152 ± 5.4 nm on the coating (Figure 1c–vi) (three individual experiments). After decreasing the pH to 5, the average size increased to 212 ± 8.1 nm, possibly due to aggregation of the disassembled TA that was ruptured in the form of flakes from the exosome surface (three individual experiments) (Figure S11, Supporting Information). To support our hypothesis that the nanofilm prevents the rupture of the plasma membrane of exosomes and keeps the exosomal membrane intact, we added RNAse to the EV solution after the pH drop to destroy any external RNA and compared the RNA quantity with the controls (Figure S12, Supporting Information). There was no significant difference, which supports our interpretation that the membrane was intact without leakage.

In addition to the biocompatible, on-demand degradation capability, the [TA-Fe^{3+}] nanofilm acted as a protective layer against UV-C irradiation by absorbing UV light, especially in the UV region of 200–300 nm (**Figure 2**a).[11a] When exosomes were exposed to UV-C light (254 nm) with 8.2 or 14 J of light power for 10 min, the particle concentration of uncoated exosomes decreased to 40.2 ± 3.4% and 12.3 ± 4.2%, respectively (three individual experiments). However, 88.3 ± 4.1% and 84 ± 5.6% of nanofilm-coated exosomes were protected (three individual experiments). Not only the number of particles but also the genomic content of the exosomes GAPDH, CD9, CD63, and CD81 mRNA were protected under UV-C exposure (Figure 2b).

Furthermore, a stability test at 37 °C for 30 h was performed to assess the stability of these cloaked exosomes under physiological conditions. The concentration decreased significantly to 13.2 ± 3.9% for uncoated exosomes, while 93 ± 5.4% of coated exosomes were protected (Figure 2c). The real-time polymerase chain reaction (PCR) results confirmed that the genetic material inside the exosomes was protected by the [TA-Fe^{3+}] nanofilm (Figure 2d). Membrane rupture (Figure S13, Supporting

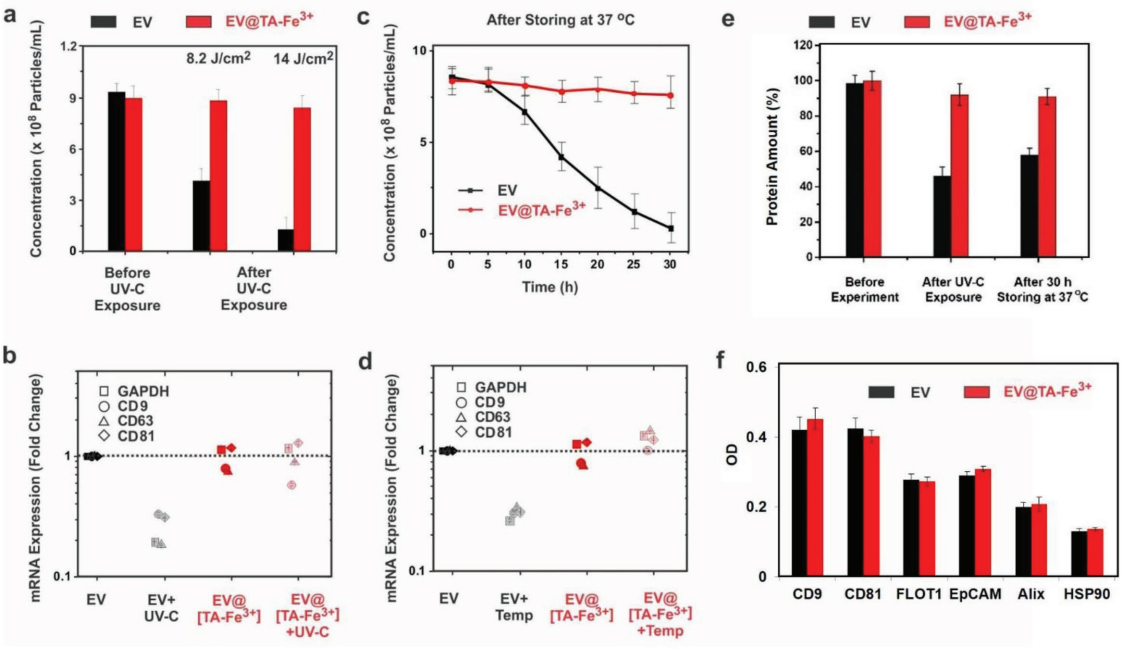

Figure 2. Enhanced tolerance of surface-protected exosomes to external stress. a) Concentration measured using NTA to test the effect of UV-C irradiation. b) mRNA quantification using real-time PCR to assess the effect of UV-C. c) Thermoprotection ability after storing at 37 °C for 30 h tested by measuring the exosome concentration using NTA. d) mRNA quantification by real-time PCR to assess degradation after storing exosomes at 37 °C for 30 h. e) Total protein analysis after UV-C irradiation and storing at 37 °C for 30 h confirmed that the nanofilm protected exosomal proteins during pH-controlled formation and degradation of polyphenol nanofilms. f) ELISA results of exosomal proteins CD9, CD81, FLOT1, EpCAM, Alix, and HSP90 from encapsulated EVs after pH shifts showed no significant differences compared to the control. All values are expressed as the mean ± SD ($n = 3$ individual experiments).

Information) and aggregation (Figure S14, Supporting Information) of the exosomes were observed under UV-C or thermal stress, whereas the [TA-Fe^{3+}] nanofilm prevented aggregation (Figure S15, Supporting Information).

In addition, we evaluated the stability of exosomal proteins. First, we performed assays to measure the amount of total proteins as shown in Figure 2e, which indicate that long-term storage and UV-C exposure reduced the protein content of the exosomes (58% and 47%, respectively; three individual experiments). In the case of cloaked exosomes, however, the exosomal protein remained similar, even after long-term storage and UV-C exposure. In addition, we also measured the exosome surface-proteins, CD9, CD81, EpCAM, and Flotillin-1 (FLOT1), and the internal proteins, Alix and HSP90, by ELISA to determine the possibility of protein degradation during the pH swing (Figure 2f). The ELISA results from native EVs and after removing polyphenol films of cloaked EVs remained similar, which suggest that the exosomal proteins are conserved during the nanofilm coating and release process.

To test the capacity for chemical functionalization, we modified EV@[TA-Fe^{3+}] with plasmonic GSH-AuNPs. Metallic nanostructures provide subwavelength localization of surface plasmon polaritons, providing a unique opportunity for imaging subdiffraction-limited structures.[14] The tripeptide GSH was chosen as a model for small molecule ligands and was readily conjugated to EV@[TA-Fe^{3+}] via Michael addition at the free amine. First, GSH-AuNPs were prepared and characterized by TEM and UV–vis spectroscopy (Figure S16, Supporting Information).[15] Next, GSH-AuNPs were covalently functionalized to EV@[TA-Fe^{3+}] and characterized by DLS (176 ± 5.7 nm) (three individual experiments). NMR (Figure S17, Supporting Information) and Raman spectroscopy (Figure S7, Supporting Information) were used to assess the chemical composition of the GSH-AuNP-modified EV@[TA-Fe^{3+}], and TEM showed GSH-AuNPs attached on the surface of EV@[TA-Fe^{3+}] (**Figure 3**a).

Together, this evidence proved that a TA coating can be used for surface functionalization of exosomes. Given that the plasmonic resonance of AuNPs is critically dependent on their interparticle distance, this phenomenon was examined by DFM.[14] GSH-AuNPs scattered green light with a very low intensity under DFM (Figure S18a, Supporting Information), but there was a marked increase in scattering intensity when they were covalently bonded to the surface of EV@[TA-Fe^{3+}] (Figure 3b). After decreasing the pH, the plasmonically coupled GSH-AuNPs dissociated from the exosome surface and were eventually released, showing a low scattering intensity (Figure 3c). The cell viability results showed that this nanobioprobe, AuNPs-decorated EV@[TA-Fe^{3+}], had negligible cytotoxic effects on MCF-7 cells (Figure 3d). We also checked the cytotoxicity of EV@[TA-Fe^{3+}] on normal cells, which showed negligible cytotoxic effects on CCD1058SK (Figure S19, Supporting Information). The nanobioprobe was relatively stable at physiological pH (7.4) and gradually disassembled at lower pH values corresponding to those in endosomal and lysosomal compartments (5.0–6.0), which is a highly desirable property for nanomedicine applications (Figure 3e).

Having established these plasmonic properties, we also assessed internalization of these cloaked exosomes in MCF-7 cells. First, 2.6×10^{11} Au-EV@[TA-Fe^{3+}] were incubated with MCF-7 cells at 37 °C for 2 h, and the excess Au-EV@[TA-Fe^{3+}] were removed by washing the cells with phosphate-buffered saline (PBS). Internalization was confirmed by the bright red-orange color inside the cells (Figure 3f), while DFM images of the untreated cells showed much weaker scattering (Figure S18b, Supporting Information). After 3 h, most of the internalized Au-EV@[TA-Fe^{3+}] remained intact, retaining their original DFM scattering intensity. With increasing incubation time (12 h), the scattering intensity of the internalized exosomes decreased to 13% due to chemical degradation of the coating at low endosomal pH (Figure 3g) (three individual experiments). This process continued with increasing incubation time, as monitored from the average scattering intensity decrease (Figure 3h) and revealed their potential as a cargo for biomolecule release, which is useful for advanced nanomedicine applications.

To reveal the exact location of this nanobioprobe inside the cells, MCF-7 cells, after 3 h of incubation with the nanoprobe, were characterized by TEM. A high-magnification TEM image revealed that the nanobioprobes were mainly located in the endosomes, indicative of endocytosis. Some of the dissociated particles were found distributed in cytosol as well (Figure 3i). In addition, we performed a live tracking experiment by using confocal reflection microscopy. The reflection images were overlaid and compared with the fluorescence images obtained with the commercially available lysosome-targeting Lysotracker, which further supports that the AuNPs-decorated EV@[TA-Fe^{3+}] is indeed present inside the lysosome of the cells (Figure 3j), providing proof-of-concept.

Furthermore, we engineered these clocked exosomes to combine the characteristics of targeted delivery of anticancer chemotherapeutics. In this experiment, we chose the chemotherapeutic doxorubicin (DOX) hydrochloride as the model drug due to its widespread clinical application. DOX loading into EV was done by electroporation, which was dependent on the drug concentration in the suspension solution: 0.29–1.72 μg of DOX was associated with 1 μg of EV (measured on the basis of total protein amount) (Figure S20, Supporting Information). To test drug release time, three in vitro experiments were performed (Figure S21, Supporting Information) showing that most of the drug was released within 3 h.

The drug-loaded EV@[TA-Fe^{3+}] was then modified with folic acid (FA) and used for preferential cellular uptake to MCF-7 cancer cells against CCD1058SK normal cells. FA-EV@[TA-Fe^{3+}]$_{DOX}$ showed sixfold higher cellular uptake to cancer cells than to normal cells, while EV_{DOX} alone produced no significant difference in cellular uptake (**Figure 4**a). To further investigate this premise of preferential targeting of cancer cell cells, a cytotoxicity test of EV_{DOX}, EV@[TA-Fe^{3+}]$_{DOX}$, and FA-EV@[TA-Fe^{3+}]$_{DOX}$ was performed using an [3-(4,5-dimethylthiazol-2-yl)-2,5-diphenyltetrazolium bromide] (MTT) assay (Figure 4b–d). At high concentrations of FA-EV@[TA-Fe^{3+}]$_{DOX}$, the cell viability of MCF-7 cells was more than threefold lower than that of CCD1058SK cells (Figure 4d). This reduced viability of MCF-7 cells was likely caused by the increased uptake of FA-EV@[TA-Fe^{3+}]$_{DOX}$ due to folate receptor–mediated endocytosis and further release of DOX from the exosomes in the intracellular compartments. However, in the case of EV_{DOX}, we could not

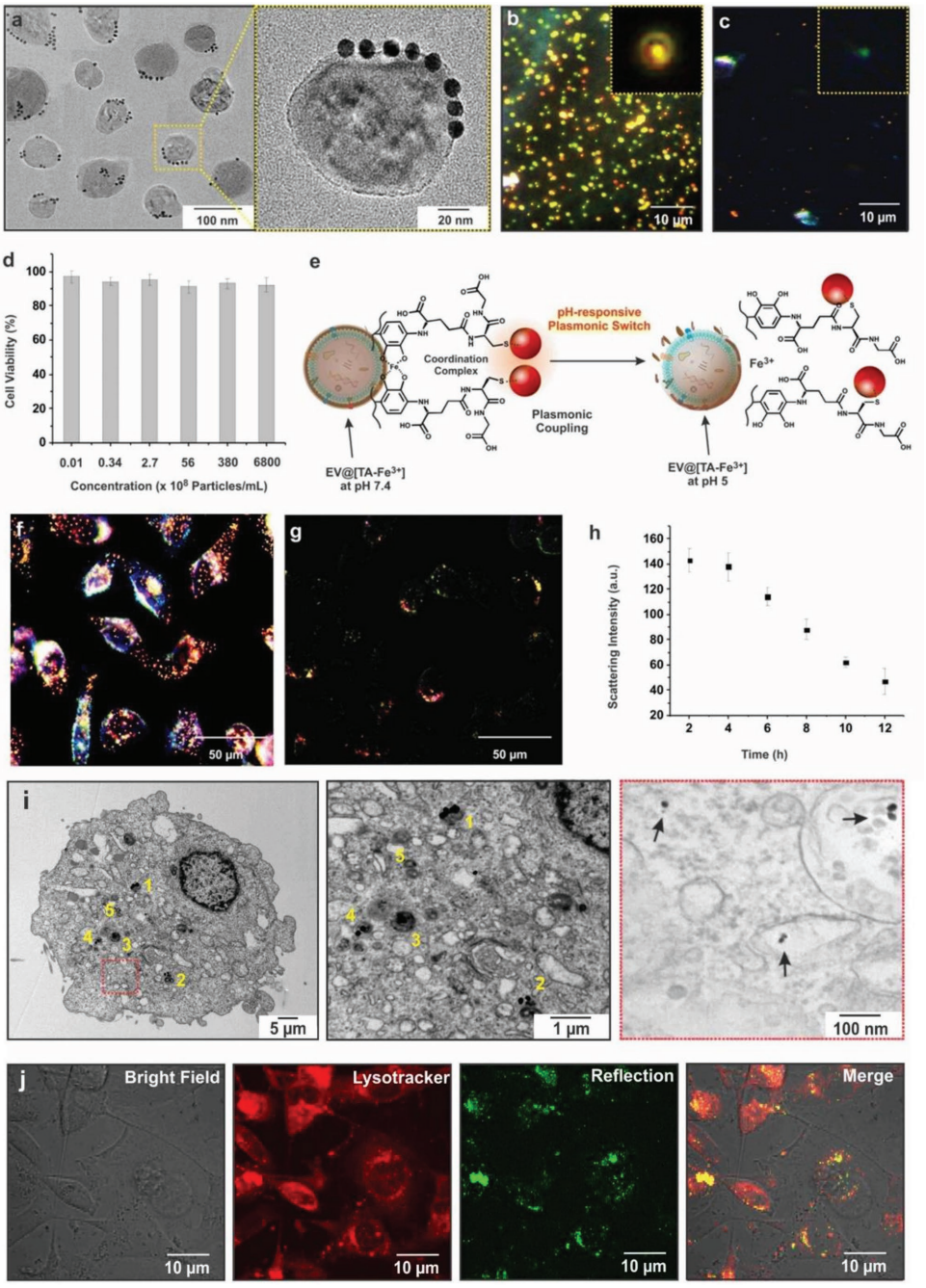

Figure 3. Surface functionalization. a) TEM images of tethered GSH-AuNPs on the exosome surfaces. b) DFM images in PBS at pH 7.4. c) DFM images after switching to pH = 5. d) MCF-7 cell viability assay after incubation with Au-EV@[TA-Fe^{3+}]. All values are expressed as the mean ± SD (n = 3 individual experiments). e) Schematic diagram showing the pH-responsive plasmonic switch. DFM images of cells after incubation for f) 2 h and g) 12 h. h) Scattering intensities of the cloaked exosomes within cells as a function of incubation time. All values are expressed as the mean ± SD (n = 3 individual experiments). i) TEM images of fixed and sectioned cells internalized with Au-EV@[TA-Fe^{3+}], high magnification TEM images of Au-EV@[TA-Fe^{3+}] in lysosomes (1,2,3,4, and 5) (middle), high magnification TEM images of GSH-AuNPs in cytoplasm (arrow) (right). j) Confocal reflection microscopy images for co-localization of Au-EV@[TA-Fe^{3+}] (green) with lysosomes (red).

see any significant difference between the cell viability of cancer and normal cells. More important than this specific example is the proof of concept, showing that approaches using [TA-Fe^{3+}] coating allow one to tailor exosomes to target specific cells with potential therapeutic antitumor efficacy.

To our knowledge, no previous studies have taken this approach to resolve the exosome encapsulation problem. The present method is simple, fast, and substrate-independent, and it generates a uniform and robust [TA-Fe^{3+}] protective shield on exosomes that imparts several useful attributes:

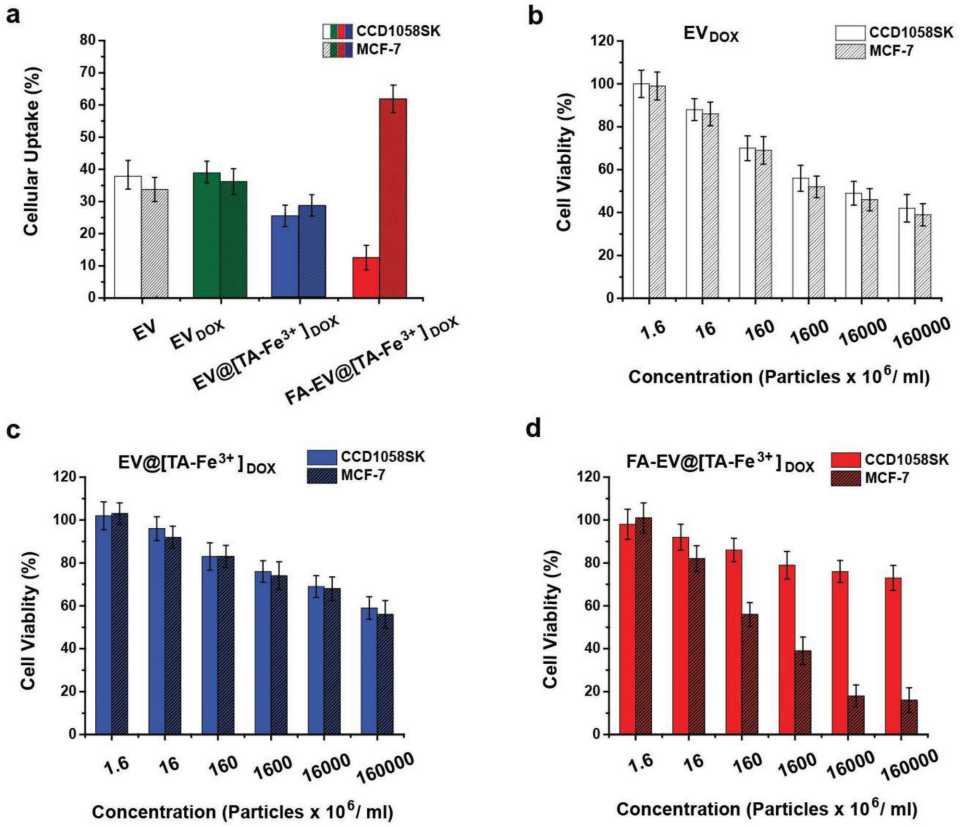

Figure 4. Targeted delivery of anticancer drug. a) Cellular uptake of EV, EV_{DOX}, EV@[TA-Fe^{3+}]$_{DOX}$ and FA-EV@[TA-Fe^{3+}]$_{DOX}$ determined by NTA. All experiments were performed in quadruplicate and with three independent repeats. The concentration-dependent cytotoxicity effects of b) EV_{DOX}, c) EV@[TA-Fe^{3+}]$_{DOX}$, and d) FA-EV@[TA-Fe^{3+}]$_{DOX}$ on MCF-7 (cancer cells) and CCD1058SK (normal cells). All values are expressed as the mean ± SD (n = 3 individual experiments).

1) Exosome protection. The [TA-Fe^{3+}] nanofilm prevents the rupture of plasma membrane of exosomes at 37 °C and protects exosomes from harmful external stresses such as UV-C irradiation;
2) On-demand degradation of the cloaking film, which is particularly important for exosome-based diagnostics that require long-term preservation of exosomes under ambient conditions;
3) Surface functionalization of the cloaking film to introduce chemical ligands or functional molecules has been demonstrated with the attachment of AuNPs and a cancer-targeting ligand. This is significant not only as a proof-of-concept, but also because this specific example provides a method that could be used to track exosome delivery or as a strategy to incorporate synergistic therapeutic agents.

This mild, easy, versatile, and scalable coating method shows the potential for exosome surface manipulation, thus extending applications of exosome-based disease theranostics.

Supporting Information

Supporting information is available from the Wiley Online Library or from the author.

Acknowledgements

This work was supported by the taxpayers of South Korea through the Institute for Basic Science (IBS-R020-D1).

Conflict of Interest

The authors declare no conflict of interest.

Keywords

exosomes, nanoencapsulation, nanofilms, surface engineering, tannic acid

Received: May 29, 2018
Published online: July 19, 2018

[1] a) H. Valadi, K. Ekstrom, A. Bossios, M. Sjostrand, J. J. Lee, J. O. Lotvall, *Nat. Cell Biol.* **2007**, *9*, 654; b) S. E. Andaloussi, I. Mager, X. O. Breakefield, M. J. A. Wood, *Nat. Rev. Drug Discovery* **2013**, *12*, 347.
[2] G. Raposo, W. Stoorvogel, *J. Cell Biol.* **2013**, *200*, 373.
[3] S. El-Andaloussi, I. Mager, X. O. Breakefield, M. J. A. Wood, *Nat. Rev. Drug Discovery* **2013**, *12*, 347.

[4] P. D. Robbins, A. E. Morelli, *Nat. Rev. Immunol.* **2014**, *14*, 195.
[5] a) H. Im, H. Shao, Y. I. Park, V. M. Peterson, C. M. Castro, R. Weissleder, H. Lee, *Nat. Biotechnol.* **2014**, *32*, 490; b) H. Woo, V. Sunkara, J. Park, T. Kim, J. Han, C. Kim, H. Choi, Y. Kim, Y. Cho, *ACS Nano* **2017**, *11*, 1360.
[6] a) J. P. K. Armstrong, M. N. Holme, M. M. Stevens, *ACS Nano* **2017**, *11*, 69; b) M. Lee, J-J Ban, W. Im, M. Kim, *Biotechnol. Bioprocess Eng.* **2016**, *21*, 299; c) Q. Ge, Y. Zhou, J. Lu, Y. Bai, X. Xie, Z. Lu, *Molecules* **2014**, *19*, 1568.
[7] a) C. P. Lai, O. Mardini, M. Ericsson, S. Prabhakar, C. A. Maguire, J. W. Chen, B. A. Tannous, X. O. Breakefield, *ACS Nano* **2014**, *8*, 483; b) M. Morishita, Y. Takahashi, A. Matsumoto, M. Nishikawa, Y. Takakura, *Biomaterials* **2016**, *111*, 55.
[8] a) R. Maroto, Y. Zhao, M. Jamaluddin, V. L. Popov, H. Wang, M. Kalubowilage, Y. Zhang, J. Lusi, H. Sun, C. T. Culbertson, S. H. Bossmann, M. Motamedi, A. R. Brasier, *J. Extracell. Vesicles* **2017**, *5*, 9799; b) X. Yu, H. Cai, W. Zhang, X. Li, N. Pan, Y. Luo, X. Wang, J. G. Hou, *ACS Nano* **2011**, *6*, 1.
[9] a) M. Wang, S. Altinoglu, Y. S. Takeda, Q. Xu, *PLoS One* **2015**, *10*, e0141860; b) I. Nakase, K. Noguchi, I. Fujii, S. Futaki, *Sci. Rep.* **2016**, *6*, 34937, 1–10; c) S. Cogoi, U. Jakobsen, E. B. Pedersen, S. Vogel, L. E. Xodo, *Sci. Rep.* **2016**, *6*, 38468, 1–13.
[10] a) H. Ejima, J. J. Richardson, K. Liang, J. P. Best, M. P. V. Koeverden, G. K. Such, J. Cui, F. Caruso, *Science* **2013**, *341*, 154; b) J. Guo, B. L. Tardy, A. J. Christofferson, Y. Dai, J. J. Richardson, W. Zhu, M. Hu, Y. Ju, J. Cui, R. R. Dagastine, I. Yarobsky, F. Caruso, *Nat. Nanotechnol.* **2016**, *11*, 1105.
[11] a) J. H. Park, K. Kim, J. Lee, J. Y. Choi, D. Hong, I. S. Choi, *Angew. Chem., Int. Ed.* **2014**, *53*, 12420; b) K. Liang, J. J. Richardson, J. Cui, F. Caruso, C. J. Doonan, P. Falcaro, *Adv. Mater.* **2016**, *28*, 7910; c) J. H. Park, D. Hong, J. Lee, I. S. Choi, *Acc. Chem. Res.* **2016**, *49*, 792; d) B. J. Kim, S. Han, K-B Lee, I. S. Choi, *Adv. Mater.* **2017**, *29*, 1700784.
[12] N. H. Andersen, M. J. Harrington, H. Birkedal, B. P. Lee, P. B. Messersmith, K. Y. C. Lee, J. H. Waite, *Proc. Natl. Acad. Sci. U. S. A.* **2011**, *108*, 2651.
[13] S. A. Melo, L. B. Luecke, C. Kahlert, A. F. Fernandez, S. T. Gammon, J. Kaye, V. S. LeBleu, E. A. Mittendorf, J. Weitz, N. Rahbari, C. Reissfelder, C. Pilarsky, M. F. Fraga, D. Piwnica-Worms, R. Kalluri, *Nature* **2015**, *523*, 177.
[14] a) Y. K. Lee, S. Kim, J-W Oh, J-M Nam, *J. Am. Chem. Soc.* **2014**, *136*, 4081; b) S. Lal, S. Link, N. J. Halas, *Nat. Photonics* **2007**, *1*, 641.
[15] S. Kumar, W-K Rhim, D-K Lim, J-M Nam, *ACS Nano* **2013**, *7*, 2221.